Spatially Variable Advection Correction of Radar Data. Part I: Theoretical Considerations

ALAN SHAPIRO

School of Meteorology, and Center for Analysis and Prediction of Storms, University of Oklahoma, Norman, Oklahoma

KATHERINE M. WILLINGHAM

Cooperative Institute for Mesoscale Meteorological Studies, University of Oklahoma, and NOAA/OAR/ National Severe Storms Laboratory, Norman, Oklahoma

COREY K. POTVIN

School of Meteorology, and Center for Analysis and Prediction of Storms, and Cooperative Institute for Mesoscale Meteorological Studies, University of Oklahoma, Norman, Oklahoma

(Manuscript received 9 February 2010, in final form 27 May 2010)

ABSTRACT

Radar data–based analysis products, such as accumulated rainfall maps, dual-Doppler wind syntheses, and thermodynamic retrievals, are prone to substantial error if the temporal sampling interval is too coarse. Techniques to mitigate these errors typically make use of advection-correction procedures (space-to-time conversions) in which the analyzed radial velocity or reflectivity field is idealized as a pattern of unchanging form that translates horizontally at constant speed. The present study is concerned with an advection-correction procedure for the reflectivity field in which the pattern-advection components vary spatially. The analysis is phrased as a variational problem in which errors in the frozen-turbulence constraint are minimized subject to smoothness constraints. The Euler–Lagrange equations for this problem are derived and a solution is proposed in which the trajectories, pattern-advection fields, and reflectivity field are analyzed simultaneously using a combined analytical and numerical procedure. The potential for solution nonuniqueness is explored.

1. Introduction

A longstanding problem in radar meteorology and hydrology is the sensitivity of radar data–based analysis products to the temporal sampling interval[1] (volume scan time). Successive volume scans of radar data are used to generate accumulated rainfall maps (e.g., Austin 1987; Fabry et al. 1994; Liu and Krajewski 1996; Fulton et al. 1998; Anagnostou and Krajewski 1999; Tabary 2007; Gerstner and Heinemann 2008; Islam and Rasmussen 2008; Villarini and Krajewski 2010), wind vectors from single-Doppler velocity retrievals (e.g., Tuttle and Foote 1990; Sun and Crook 1994, 2001; Laroche and Zawadzki 1995; Shapiro et al. 1995, 2003; Zhang and Gal-Chen 1996; Liou 1999; Liou and Luo 2001; Lazarus et al. 2001; Gao et al. 2001; Xu et al. 2001a,b; Caya et al. 2002), multiple-Doppler wind and vertical velocity analyses (e.g., Clarke et al. 1980; Miller and Kropfli 1980; Ray et al. 1980; Gal-Chen 1982; Chong et al. 1983; Mohr et al. 1986), multiple-Doppler thermodynamic retrievals (e.g., Gal-Chen 1978; Hane et al. 1981; Roux 1985; Parsons et al. 1987; Sun and Houze 1992; Crook 1994; Liou 2001), and multiple-radar merged reflectivity analyses (Germann and Zawadzki 2002; Lakshmanan et al. 2006; Langston et al. 2007; Yang et al. 2009). Many of these algorithms are prone to substantial error if

[1] Operational weather radars such as the Weather Surveillance Radar-1988 Doppler (Crum and Alberty 1993; Klazura and Imy 1993) or Terminal Doppler Weather Radar (Michelson et al. 1990; Vasiloff 2001; NOAA/NWS 2005) typically scan a preset sequence of 360° conical surfaces comprising a volume of the atmosphere every 4–10 min. Research weather radars such as the Phased Array Radar (PAR; Zrnic et al. 2007; Lu and Xu 2009), the Shared Mobile Atmospheric Research and Teaching Radar (SMART-R; Biggerstaff et al. 2005) and the Doppler-on-Wheels (DoW; Wurman et al. 1997) have more flexible sampling strategies that can provide volume updates on the order of a minute over limited azimuthal sectors.

Corresponding author address: Alan Shapiro, School of Meteorology, University of Oklahoma, 120 David L. Boren Blvd., Room 5900, Norman, OK 73072.
E-mail: ashapiro@ou.edu

DOI: 10.1175/2010JAS3465.1

advection effects are not adequately accounted for or if the evolution time scale is comparable to (or smaller than) the temporal sampling interval, as might occur when a convective storm undergoes rapid changes in size, shape, or intensity.

Attempts to mitigate analysis errors arising from the nonsimultaneity of the data collection have largely focused on the advection problem. Advection-correction procedures are based on the hypothesis that, for sufficiently short time intervals, small-scale features can be idealized as patterns of unchanging form that translate horizontally (the frozen-turbulence hypothesis; Taylor 1938). In most applications, the Cartesian advection components U and V are treated as constants within an analysis domain or subdomain and are used to spatially shift nonsimultaneously gathered data on an observational grid to an analysis grid at a common analysis time. Equivalently, a moving reference frame is introduced in which the analysis is performed.

A variety of techniques have been used to estimate U and V. They have been obtained subjectively, by visually tracking echo cores or shear lines (Heymsfield 1978; Carbone 1982; Austin 1987; Dowell and Bluestein 1997), and objectively, by cross-correlation analysis (Zawadzki 1973; Austin and Bellon 1974; Mohr et al. 1986; Anagnostou and Krajewski 1999, Gerstner and Heinemann 2008), by minimizing a cost function in which the frozen turbulence hypothesis or a related hypothesis is imposed as a weak constraint (Gal-Chen 1982; Chong et al. 1983; Shapiro et al. 1995; Zhang and Gal-Chen 1996; Liou 1999; Liou and Luo 2001; Lazarus et al. 2001, Matejka 2002; Dowell and Bluestein 2002), and by determining the reference frame that yields the most dynamically consistent pressure and buoyancy fields in a thermodynamic retrieval (Hane 1993). Some wind retrieval algorithms simultaneously effect advection correction and wind retrieval, with the advection components determined as part of the overall analysis procedure (Caillault and Lemaitre 1999; Caya et al. 2002). Finally, we note that advection components in convective storms can, in principle, be obtained from storm-tracking algorithms (Rosenfeld 1987; Dixon and Wiener 1993; Johnson et al. 1998; Andrejczuk et al. 2003; Lakshmanan et al. 2003; Yang et al. 2009).

The frozen-turbulence hypothesis as applied to the reflectivity field R appears as

$$\frac{DR}{Dt} = 0, \tag{1.1}$$

or, equivalently, with the total derivative operator D/Dt expanded in Eulerian form,

$$\frac{\partial R}{\partial t} + U\frac{\partial R}{\partial x} + V\frac{\partial R}{\partial y} = 0. \tag{1.2}$$

As shown by Gal-Chen (1982, section 2a), the U and V parameters (constants) that minimize the squared error in (1.2) satisfy two linear algebraic equations whose coefficients are products of the space and time derivatives of R integrated over a four-dimensional (spatiotemporal) analysis domain. However, Gal-Chen found that in order for the solution of those linear algebraic equations to yield accurate values for U and V, it was necessary to proceed iteratively, with the coefficients updated with improved (advection-corrected) estimates of the local derivative. Since accurate estimation of the local derivative is required for accurate estimation of U and V (and vice versa), the coefficients are implicitly functions of U and V, and thus the ''linear'' algebraic equations are, in fact, nonlinear. The potential for nonuniqueness of this method was noted by Protat and Zawadzki (1999).

When applied to the velocity field $\mathbf{u}$, the frozen-turbulence hypothesis appears as $D\mathbf{u}/Dt = 0$, with analogous expressions for the Cartesian velocity components. Unfortunately, an analogous expression does not hold for the radial wind field v_r because v_r varies with the sampling angle[2] (in addition to the velocity field). However, as shown by Gal-Chen (1982), if $\mathbf{u}$ satisfies the frozen-turbulence hypothesis, then v_r satisfies

$$\frac{D^2(rv_r)}{Dt^2} = 0, \tag{1.3}$$

with the corresponding least squares minimization problem yielding two nonlinear algebraic equations for U and V. As in the reflectivity-based approach, accurate estimation of the local derivatives appearing in the coefficients in the algebraic equations may require that one contend with coefficients that depend implicitly on U and V.

Once U and V have been estimated (e.g., through least squares error minimization of a frozen-turbulence constraint or through a subjective process), radar data can be advected forward or backward in time along pattern trajectories to an analysis grid at a common analysis time. The advection step typically uses a strong-constraint form of the frozen-turbulence equation: for example, (1.1),

[2] Consider a zone of air characterized by uniform westerly winds (u is constant and positive; v is zero) that advects eastward. When this zone is probed west of the radar, v_r is negative, but when the same zone is probed when it is east of the radar, v_r is positive. Thus, v_r in the zone changes even though the velocity field in the zone does not change.

which integrates to R = constant following the motion of the pattern (storm). Alternatively, a linear time interpolation formula can be used in conjunction with a Lagrangian or moving reference frame analysis (e.g., Protat and Zawadzki 1999; Liu et al. 2004).

A drawback of treating advection parameters as constants in an advection-correction procedure is that analyzed features in regions where the true advection velocity varies considerably may become distorted or shifted relative to their correct locations. This problem may be acute in the analysis of tornados and other small-scale vortices in high-resolution datasets in which a feature of interest (e.g., a tornado) can be advected by a mesocyclone or other nonuniform mesoscale flow.

In this study we introduce an advection-correction technique for radar reflectivity data in which the advection components in the frozen-turbulence constraint (1.2) vary spatially but are independent of time (although an extension of the procedure to include time dependence in the advection components is outlined in the appendix). The procedure can, in principle, be applied to reflectivity data from Doppler or non-Doppler radars or to microwave or infrared brightness temperature data from satellites.

The underpinning of the proposed advection-correction procedure (minimization of a cost function in which a frozen-turbulence constraint is imposed) is similar to that of many of the aforementioned single-Doppler velocity retrieval algorithms,[3] and especially to that of the variational echo tracking (VET) procedure (Laroche and Zawadzki 1995). The main differences are in philosophy, intended application, and some technical details. In a single-Doppler velocity retrieval, the analyzed field of interest is the wind field (U, V are interpreted as true velocity components), and the reflectivity and/or radial velocity field is treated as a marker for the flow (i.e., used as a means to infer the velocity components). For the purpose of advection correction, however, U and V are interpreted as pattern-advection components (not necessarily velocity components of air parcels), and the focus is on analyzing the reflectivity and/or radial velocity fields. The distinction between the two interpretations is apparent if we consider, for example, westerly flow through a stationary orographic thunderstorm. Since the storm is stationary, the pattern-advection U, V components are zero, while air parcels flowing through the storm have a nonzero westerly velocity component. We conjecture that in many circumstances, frozen-turbulence-based single-Doppler velocity retrieval techniques may actually work better as advection-correction procedures than as wind retrieval algorithms. In any case, the computer codes for many single-Doppler velocity retrievals can, in principle, be adapted to serve as advection-correction procedures.

A VET formalism was also applied by Germann and Zawadzki (2002) to the problem of precipitation nowcasting. In that application, as in our study, the U, V fields are treated as pattern-advection components rather than velocity components. However, whereas Germann and Zawadzki (2002) were concerned with the extrapolation of reflectivity observations, which is a forecasting problem, we are concerned with the use of an interpolative procedure to effect the advection correction of nonsimultaneous data, which is an analysis problem.

The plan of Part I of this study is as follows. In section 2 the analysis is phrased as a variational problem in which errors in (1.2) are minimized subject to smoothness constraints. In sections 3 and 4, a minimization procedure is proposed to simultaneously determine spatially variable advection fields and analyze the reflectivity field. The potential solution nonuniqueness for a fairly general analysis procedure that includes the Gal-Chen (1982) reflectivity-based algorithm, the VET procedure, and the new advection correction method as special cases is discussed in section 5. Section 5 also serves to verify that the main numerical modules for the new method are free of code errors. In Part II of this study (Shapiro et al. 2010, hereafter Part II), the new method is tested using analytical data of reflectivity blobs embedded within a solid body vortex and real Terminal Doppler Weather Radar (TDWR) and Weather Surveillance Radar-1988 Doppler (WSR-88D) data of a supercell thunderstorm.

2. Problem statement

Consider an analysis volume comprised of a set of two-dimensional surfaces, which may be surfaces of constant elevation angle (conical surfaces or sectors of conical surfaces) or surfaces of constant height. Following the naming convention for displays of radar data, we will refer to these surfaces as plan position indicators (PPIs) and constant altitude plan position indicators (CAPPIs), respectively. The analysis proceeds on one PPI or CAPPI surface at a time. A Cartesian (x, y) analysis grid is embedded on each surface. Reflectivity data are interpolated from the observation points on the native spherical grid to the analysis grid. In a PPI analysis, U and V are quasi-horizontal advection components accounting for pattern advection on a conical surface, whereas in a CAPPI analysis U and V are true horizontal advection components. In the latter case, however, data from two or more elevation angles are required for the interpolation.

[3] Our discussion here refers to single-Doppler velocity retrievals based on a frozen-turbulence constraint and not on retrievals based on the full equation set of a numerical weather prediction model.

Such interpolation invariably carries with it errors due to nonsimultaneity of the data, but these can be limited if the number of elevation angles used in the interpolation to any height surface is small (it may be desirable to restrict the analysis to low elevation angles or limit the lateral extent of an analysis surface so that it is bounded above and below by the same two scan angles). After the data are interpolated to an analysis surface, the surface is given a time stamp indicating the valid time of the data on that surface.

The advection correction/analysis procedure uses data from two consecutive volume scans. If T is the time interval between these scans, we can denote the two consecutive valid times of the data on the ith analysis surface as t_i and $t_i + T$. We refer to these as CAPPI times (or PPI times). Since it will be necessary to integrate and differentiate certain quantities with respect to time at analysis points and along trajectories running through analysis points, we will consider a range of computational times between the two CAPPI times (Fig. 1). The advection-corrected/analyzed field will be available at all of the computational times, so we may refer to them interchangeably as analysis times or computational times. In practice, we may only be interested in the analysis at one of those times.

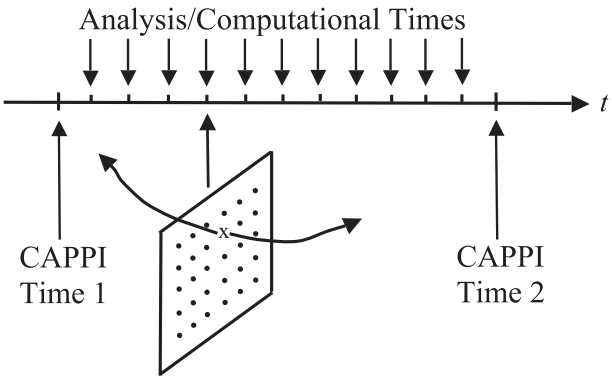

FIG. 1. Schematic illustrating the analysis grid at one of the analysis/computational times with a forward and backward trajectory running through one of the analysis points at that time (marked with x). Forward and backward trajectories are launched from every analysis point at every analysis/computational time. Data from the second CAPPI time are interpolated to forward trajectories; data from the first CAPPI time are interpolated to backward trajectories.

Our analysis problem is posed as follows. We seek $U(x, y)$, $V(x, y)$, and $R(x, y, t)$ fields that minimize a cost function in which the frozen-turbulence hypothesis (1.2) and spatial smoothness (penalty) terms are imposed as weak (least squares error) constraints,

$$J \equiv \iiint \left[\alpha \left(\frac{\partial R}{\partial t} + U \frac{\partial R}{\partial x} + V \frac{\partial R}{\partial y} \right)^2 + \beta \left| \nabla_h U \right|^2 + \beta \left| \nabla_h V \right|^2 \right] dx\, dy\, dt, \tag{2.1}$$

with reflectivity data incorporated at the two CAPPI times t_i and $t_i + T$. Here ∇_h is the horizontal gradient operator, and the integration domain extends over the ith analysis surface and over the time window between the two CAPPI times. The first-derivative smoothness terms act as low-pass filters for noise suppression and also provide smooth interpolation of U and V fields across reflectivity data voids (Sasaki 1970, 1971). For our purposes, however, the smoothness terms are the primary means of obtaining gradually varying "large-scale" U, V fields suitable for advecting the smaller-scale features in the data. Such smoothness terms are not included for the reflectivity field because we wish to preserve, as much as possible, the small-scale features and large gradients present in the data (although a small amount of explicit smoothing designed to remove grid-scale noise was beneficial in the tests in Part II).

The parameter β in (2.1) is a constant positive weighting coefficient. The determination of an acceptable value for β in any given application will likely require some experimentation and the analyst's intuition concerning what is desirable or acceptable in the final result. However, if one reasons that the smoothness terms should be a small fraction ε of the frozen-turbulence term, then scale analysis yields a crude provisional estimate $\beta \sim \varepsilon R_c^2$, where R_c is a reflectivity scale. For example, if one takes $R_c \sim 50$ dBZ (e.g., in a convective storm) and considers the smoothness terms to be ~10% of the magnitude of the frozen-turbulence term ($\varepsilon \sim 0.1$), then β is on the order of a few hundred dBZ^2.

The variable $\alpha = \alpha(x, y, t)$ in (2.1) is a binary (0, 1) analysis coverage function (footprint function). Because of the inhomogeneous distributions and densities of the scatterers, the footprint of data coverage on an analysis surface is usually less than the actual area of that surface. When viewed in PPI/CAPPI imagery, this footprint often appears as a pattern translating across the screen. The specification of α will be described in section 3.

3. Minimization of the cost function

To minimize J, we apply basic concepts from the calculus of variations (e.g., Lanczos 1986; Courant and Hilbert 1953). Setting the variation of J to zero, we obtain

$$\iiint\left[\alpha\left(\frac{\partial R}{\partial t}+U\frac{\partial R}{\partial x}+V\frac{\partial R}{\partial y}\right)\left(\frac{\partial \delta R}{\partial t}+U\frac{\partial \delta R}{\partial x}+V\frac{\partial \delta R}{\partial y}+\delta U\frac{\partial R}{\partial x}+\delta V\frac{\partial R}{\partial y}\right)+\beta\left(\frac{\partial U}{\partial x}\frac{\partial \delta U}{\partial x}+\frac{\partial U}{\partial y}\frac{\partial \delta U}{\partial y}\right.\right.$$
$$\left.\left.+\frac{\partial V}{\partial x}\frac{\partial \delta V}{\partial x}+\frac{\partial V}{\partial y}\frac{\partial \delta V}{\partial y}\right)\right]dx\,dy\,dt=0. \tag{3.1}$$

Evaluating (3.1) for the arbitrary and independent variations δU, δV, and δR will lead to a set of differential equations (Euler–Lagrange equations) for U, V, and R. Toward that end, we integrate (3.1) by parts so that δU, δV, and δR appear only in undifferentiated form. We then obtain

$$I_{tb}+I_{xb}+I_{yb}+I_{\delta R}+I_{\delta U}+I_{\delta V}=0, \tag{3.2}$$

where I_{tb}, I_{xb}, and I_{yb} are boundary integrals,

$$I_{tb}\equiv\iint\left[\alpha\left(\frac{\partial R}{\partial t}+U\frac{\partial R}{\partial x}+V\frac{\partial R}{\partial y}\right)\delta R\right]_{t_i}^{t_i+T}dx\,dy, \tag{3.3a}$$

$$I_{xb}\equiv\iint\left[\alpha U\left(\frac{\partial R}{\partial t}+U\frac{\partial R}{\partial x}+V\frac{\partial R}{\partial y}\right)\delta R+\beta\left(\frac{\partial U}{\partial x}\delta U+\frac{\partial V}{\partial x}\delta V\right)\right]_{x_1}^{x_2}dy\,dt, \tag{3.3b}$$

$$I_{yb}\equiv\iint\left[\alpha V\left(\frac{\partial R}{\partial t}+U\frac{\partial R}{\partial x}+V\frac{\partial R}{\partial y}\right)\delta R+\beta\left(\frac{\partial U}{\partial y}\delta U+\frac{\partial V}{\partial y}\delta V\right)\right]_{y_1}^{y_2}dx\,dt, \tag{3.3c}$$

and $I_{\delta U}$, $I_{\delta V}$, and $I_{\delta R}$ are integrals spanning the spatiotemporal analysis domain,

$$I_{\delta U}\equiv\iiint\left[\alpha\frac{\partial R}{\partial x}\left(\frac{\partial R}{\partial t}+U\frac{\partial R}{\partial x}+V\frac{\partial R}{\partial y}\right)-\beta\left(\frac{\partial^2 U}{\partial x^2}+\frac{\partial^2 U}{\partial y^2}\right)\right]\delta U\,dx\,dy\,dt, \tag{3.4a}$$

$$I_{\delta V}\equiv\iiint\left[\alpha\frac{\partial R}{\partial y}\left(\frac{\partial R}{\partial t}+U\frac{\partial R}{\partial x}+V\frac{\partial R}{\partial y}\right)-\beta\left(\frac{\partial^2 V}{\partial x^2}+\frac{\partial^2 V}{\partial y^2}\right)\right]\delta V\,dx\,dy\,dt, \tag{3.4b}$$

$$I_{\delta R}\equiv-\iiint\left[\alpha\left(\frac{\partial}{\partial t}+U\frac{\partial}{\partial x}+V\frac{\partial}{\partial y}\right)^2R+\alpha\left(\frac{\partial U}{\partial x}+\frac{\partial V}{\partial y}\right)\left(\frac{\partial R}{\partial t}+U\frac{\partial R}{\partial x}+V\frac{\partial R}{\partial y}\right)\right.$$
$$\left.+\left(\frac{\partial \alpha}{\partial t}+U\frac{\partial \alpha}{\partial x}+V\frac{\partial \alpha}{\partial y}\right)\left(\frac{\partial R}{\partial t}+U\frac{\partial R}{\partial x}+V\frac{\partial R}{\partial y}\right)\right]\delta R\,dx\,dy\,dt. \tag{3.4c}$$

Since U and V are treated as independent of time, and the time integration extends over an interval T, (3.4a) and (3.4b) can be rewritten as

$$I_{\delta U}\equiv\iint\left[\int\alpha\frac{\partial R}{\partial t}\frac{\partial R}{\partial x}\,dt+U\int\alpha\left(\frac{\partial R}{\partial x}\right)^2dt+V\int\alpha\frac{\partial R}{\partial x}\frac{\partial R}{\partial y}\,dt-\beta T\left(\frac{\partial^2 U}{\partial x^2}+\frac{\partial^2 U}{\partial y^2}\right)\right]\delta U\,dx\,dy, \tag{3.5a}$$

$$I_{\delta V}\equiv\iint\left[\int\alpha\frac{\partial R}{\partial t}\frac{\partial R}{\partial y}\,dt+U\int\alpha\frac{\partial R}{\partial x}\frac{\partial R}{\partial y}\,dt+V\int\alpha\left(\frac{\partial R}{\partial y}\right)^2dt-\beta T\left(\frac{\partial^2 V}{\partial x^2}+\frac{\partial^2 V}{\partial y^2}\right)\right]\delta V\,dx\,dy. \tag{3.5b}$$

Consider first the vanishing of the boundary integrals. From (3.3a) we see that I_{tb} vanishes if each analysis point is subject to one of three conditions (may be applied independently at each CAPPI time):

(i) $\alpha = 0$. No estimate of R is sought (e.g., due to locally insufficient data coverage).
(ii) $\alpha = 1$ and $\delta R = 0$. An estimate of R is sought and there is sufficient data coverage for that estimate

(R is known, so no variation of it is considered; $\delta R = 0$).

(iii) $\alpha = 1$ and $\partial R/\partial t + U\partial R/\partial x + V\partial R/\partial y = 0$ (natural boundary condition[4] for R). An estimate of R is sought but there is insufficient data coverage for a direct estimate. The natural boundary condition permits data to be advected to this location from the other CAPPI time (if available).

For the boundary integrals in (3.3b) and (3.3c), the terms multiplying δU, δV, and δR must vanish separately since these variations are arbitrary and independent of each other. Since U and V are unknown, δU and δV should not be set to 0. Instead, we impose the natural boundary condition that the normal derivatives of U and V vanish on the boundaries, that is, $\partial U/\partial x = \partial V/\partial x = 0$ on eastern and western boundaries and $\partial U/\partial y = \partial V/\partial y = 0$ on northern and southern boundaries. For the terms associated with δR, we note that since the time integration extends between the two CAPPI times (an interval over which data are not sampled), δR should not be set to 0. We thus subject each location on a lateral boundary to one of two conditions:

(i) $\alpha = 0$. No estimate of R is sought.

(ii) $\alpha = 1$ and $\partial R/\partial t + U\partial R/\partial x + V\partial R/\partial y = 0$. A local estimate of R is sought via the natural boundary condition (an advection condition) when a trajectory on which an estimate of R is available at a CAPPI time leaves the domain at some time between the two CAPPI times.

Next, consider $I_{\delta R}$, $I_{\delta U}$, and $I_{\delta V}$. Since δU, δV, and δR are arbitrary and independent of each other, the sum of terms enclosed by the square brackets in (3.4c), (3.5a), and (3.5b) should vanish identically. We thus obtain two coupled linear elliptic partial differential equations for U and V,

$$\frac{\partial^2 U}{\partial x^2} + \frac{\partial^2 U}{\partial y^2} - \frac{1}{\beta T}\left[\int \alpha \frac{\partial R}{\partial t}\frac{\partial R}{\partial x}\,dt + U\int \alpha\left(\frac{\partial R}{\partial x}\right)^2 dt + V\int \alpha \frac{\partial R}{\partial x}\frac{\partial R}{\partial y}\,dt\right] = 0, \tag{3.6a}$$

$$\frac{\partial^2 V}{\partial x^2} + \frac{\partial^2 V}{\partial y^2} - \frac{1}{\beta T}\left[\int \alpha \frac{\partial R}{\partial t}\frac{\partial R}{\partial y}\,dt + U\int \alpha \frac{\partial R}{\partial x}\frac{\partial R}{\partial y}\,dt + V\int \alpha\left(\frac{\partial R}{\partial y}\right)^2 dt\right] = 0, \tag{3.6b}$$

and a parabolic equation for R,

$$\alpha\left(\frac{\partial}{\partial t} + U\frac{\partial}{\partial x} + V\frac{\partial}{\partial y}\right)^2 R + \alpha\left(\frac{\partial U}{\partial x} + \frac{\partial V}{\partial y}\right)\left(\frac{\partial R}{\partial t} + U\frac{\partial R}{\partial x} + V\frac{\partial R}{\partial y}\right) + \left(\frac{\partial \alpha}{\partial t} + U\frac{\partial \alpha}{\partial x} + V\frac{\partial \alpha}{\partial y}\right)\left(\frac{\partial R}{\partial t} + U\frac{\partial R}{\partial x} + V\frac{\partial R}{\partial y}\right) = 0. \tag{3.6c}$$

The characteristics of (3.6c) are the curves defined by the solutions $x = x(t)$ and $y = y(t)$ of the ordinary differential equations $Dx/Dt = U(x, y)$ and $Dy/Dt = V(x, y)$. These differential equations resemble traditional trajectory equations for air parcels, but since U and V are the advection components of a geometrical feature (reflectivity pattern) rather than the velocity components of an air parcel, the characteristics are not true trajectories. For the sake of brevity, however, we will refer to the characteristics as trajectories and refer to the motion of elements of a pattern along the characteristics as motion of parcels.

We constrain the binary (0 or 1) footprint function α to satisfy the advection equation,

$$\frac{\partial \alpha}{\partial t} + U\frac{\partial \alpha}{\partial x} + V\frac{\partial \alpha}{\partial y} = 0, \tag{3.7}$$

that is, $D\alpha/Dt = 0$. Thus, α is 0 or 1 all along a trajectory. One can consider (at least) two procedures for specifying α. In method 1—the method used in our tests—α is set to 0 along a trajectory if data are missing on the trajectory at the first and/or second CAPPI time or if the trajectory leaves the analysis domain. Only if data are available on a trajectory at both CAPPI times is α set to 1. In this conservative method, a data void present at the first or second CAPPI times advects forward or backward in time along trajectories running through it. If such a trajectory ends in a region of data coverage, then the good data at that location are orphaned. Thus, not all available data may be used in the analysis, and the effective data coverage may be less than the actual data coverage at either CAPPI time. In method 2, α is only set to 0 along a trajectory if data are missing on the

[4] A natural boundary condition is a boundary condition that arises "naturally" (i.e., can be deduced) as a property of the minimization problem. For our problem, the natural boundary conditions turn out to be Neumann conditions on U and V and an advection condition on R.

trajectory at both CAPPI times. If data are available at either CAPPI time (or both), then α is set to 1. No data are orphaned in this less conservative approach. If data are missing on the trajectory at one CAPPI time, the data void is subject to the natural boundary condition $\partial R/\partial t + U\partial R/\partial x + V\partial R/\partial y = 0$, as in the evaluation of I_{tb}.

Applying (3.7) in (3.6c) and expressing the result in characteristic (trajectory) coordinates, we obtain

$$\alpha \frac{D^2R}{Dt^2} + \alpha\left(\frac{\partial U}{\partial x} + \frac{\partial V}{\partial y}\right)\frac{DR}{Dt} = 0. \tag{3.8}$$

For trajectories along which $\alpha = 0$, (3.8) is identically satisfied ($0 = 0$), and no information about R is recovered; that is, R is not analyzed. For trajectories along which $\alpha = 1$, (3.8) can be solved for DR/Dt as

$$\frac{DR}{Dt} = A \exp\left[-\int_{t_i}^{t}\left(\frac{\partial U}{\partial x} + \frac{\partial V}{\partial y}\right)dt'\right], \tag{3.9}$$

where A is a constant of integration. Integration of (3.9) with respect to time along a trajectory then yields a formula for R involving two constants of integration. Using the data at the two CAPPI times to evaluate the constants of integration, we obtain an analysis formula for R as

$$R(t) = R(t_i) + [R(t_i + T) - R(t_i)]\frac{I(t)}{I(t_i + T)}, \tag{3.10}$$

where

$$I(t) \equiv \int_{t_i}^{t} \exp\left[-\int_{t_i}^{t'} \mathrm{div}(t'')\,dt''\right]dt', \quad \mathrm{div} \equiv \frac{\partial U}{\partial x} + \frac{\partial V}{\partial y}. \tag{3.11}$$

Had we used method 2 for the evaluation of α, then in cases where data were available on a trajectory at both CAPPI times we would recover (3.10) and (3.11), but if data were missing at one of the CAPPI times then application of the natural boundary condition ($DR/Dt = 0$) in (3.9) would yield $A = 0$, and thus $R(t)$ = constant along that trajectory.

We draw attention to several aspects of the procedure:

(i) The integrals in (3.6a) and (3.6b) are evaluated at fixed locations (Eulerian sense) whereas those in (3.11) are evaluated along trajectories (Lagrangian sense). Although U and V (and hence div) are considered to be in a steady state, they may well vary with time in a Lagrangian sense since they vary spatially and so are not constant in the integrals in (3.11).

(ii) If the horizontal divergence div vanishes all along a trajectory, (3.10) reduces to a standard linear interpolation formula, $R(t) = R(t_i) + [R(t_i + T) - R(t_i)](t - t_i)/T$.

(iii) The U and V fields are obtained throughout the analysis domain, even in regions where R is not analyzed (data voids). In regions where $\alpha = 0$, (3.6a) and (3.6b) reduce to Laplace's equations for U and V. According to the maximum principle for Laplace's equation, U and V have the desirable property that within these voids they are smooth functions without local extrema (Flanigan 1983).

(iv) Although this procedure was described in continuous form, in real applications it must be implemented in discretized form. The discretization and other computational details are discussed next.

4. Computational considerations

Equations (3.6a), (3.6b), (3.7), (3.10), and (3.11) are solved by iterating between updates of R and updates of U and V. The $(n + 1)$th pass through the overall procedure begins with the nth estimates available for U, V, and R on the analysis grid. Equations (3.6a) and (3.6b) subject to zero-normal-gradient boundary conditions are then solved for the updated $[(n + 1)\text{th}]$ U, V fields using successive relaxation. It can be shown that the solution of (3.6a) and (3.6b) subject to zero-normal-gradient boundary conditions is unique during any single pass through the procedure, that is, with the R field held fixed (although as discussed in section 5, uniqueness of the overall procedure—that is, with the R field continually updating—cannot be guaranteed). The updated U, V, and div fields are then used in the trajectory analysis. At each computational time and at each analysis point, trajectories are launched forward and backward in time. The trajectories are calculated using a fourth-order Runge–Kutta technique (Press et al. 1992), with the $(n + 1)$th U, V, and div fields bilinearly interpolated from analysis grid points to points along the trajectories. Each forward trajectory is tracked until the second CAPPI time or until the trajectory leaves the analysis domain, and each backward trajectory is tracked until the first CAPPI time or until it leaves the analysis domain. If an analysis surface has N grid points and there are M computational times between the two CAPPI times, then NM forward trajectories and NM backward trajectories are calculated over the course of an analysis time window. For each analysis point and

computational time, the corresponding parcel locations $x(t), y(t)$ along the full trajectory (combined forward and backward) are noted and stored. Reflectivity data are bilinearly interpolated to the end points of the trajectory (i.e., at the two CAPPI times), if available. If radial velocity data are to be analyzed, these data are also interpolated to the end points of the trajectory. The footprint function α is then evaluated on the trajectory as $\alpha = 0$ or 1, following method 1. The solution for the updated $[(n + 1)\text{th}]$ R field along a trajectory then follows from (3.10) and (3.11). The iterations continue until differences between successive estimates of the U, V and R fields are less than specified thresholds. Since the successive relaxation module is itself an iterative algorithm, the overall analysis procedure is "doubly iterative." When discussing convergence thresholds we will make a distinction between the convergence threshold for the successive relaxation module and the convergence threshold for the overall procedure.

5. Solution nonuniqueness

As discussed in section 1, Gal-Chen's (1982) reflectivity-based advection-correction procedure leads to two linear algebraic equations for U and V whose coefficients are integrals of products of the spatial and local derivatives of R. However, since the estimates of the spatial and local derivatives themselves may be sensitive to the advection correction, the coefficients are implicitly functions of U and V. Gal-Chen proposed an iterative procedure in which U and V are continually reevaluated based on an advection-corrected reflectivity field, which itself is continually recalculated using updated U and V estimates. The problem is nonlinear, and the solution of the linear algebraic equations is merely formal. In this section we show that the reflectivity-based analysis problem considered by Gal-Chen, the VET problems considered by Laroche and Zawadzki (1995) and Germann and Zawadzki (2002), and the spatially variable advection correction problem now under consideration may have multiple solutions, even in the most optimistic scenario of data quality and spatial coverage. Local minima in the analysis cost functions were noted in the real-data experiments of Laroche and Zawadzki (1995) and Germann and Zawadzki (2002). Here we find that a fairly general class of advection-correction/analysis procedures may be subject to nonuniqueness. The proof identifies an idealized flow for which there are an infinite number of solutions satisfying all of the analysis constraints.

Consider a class of advection-correction/analysis procedures based on minimization of the cost function

$$M \equiv \int \left[\alpha \left(\frac{\partial R}{\partial t} + U \frac{\partial R}{\partial x} + V \frac{\partial R}{\partial y} \right)^2 + \sum_{j=1}^{P} \beta_j |L_j(U)|^2 + \sum_{j=1}^{P} \beta_j |L_j(V)|^2 \right] d\Omega, \tag{5.1}$$

with reflectivity data incorporated from two successive volume scans. Here P is the number of smoothness constraints, β_j is the weighting coefficient for the jth smoothness constraint, and L_j is any linear constant-coefficient differential operator (in space and/or time) of any order. The Gal-Chen algorithm corresponds to the case in which no smoothness constraints are imposed (all β_j are zero) and Ω is a four-dimensional analysis domain (volume and time). Our spatially variable advection correction algorithm corresponds to the case where $\beta_1 = \beta_2 \neq 0$ with all other β_j being zero, $L_1 = \partial/\partial x$, $L_2 = \partial/\partial y$, and Ω is a three-dimensional analysis domain (area and time). The cost functions underlying the VET methods of single-Doppler velocity retrieval (Laroche and Zawadzki 1995) and precipitation echo motion analysis (Germann and Zawadzki 2002) are also particular cases of (5.1).

Consider a true reflectivity field in the form of a wave propagating in the x direction, $R(x, y, t) = A \exp[-(ky)^2] \cos[k(x - U_{\text{true}}t)]$, where the amplitude A, wavenumber k, and advection speed U_{true} are constant. With this reflectivity field sampled at two CAPPI times, $t = 0$ and $t = T$, the input data become

$$R_0 = A \exp[-(ky)^2] \cos(kx) \quad \text{and}$$
$$R_T = A \exp[-(ky)^2] \cos[k(x - U_{\text{true}}T)]. \tag{5.2}$$

These data are considered in their exact form (5.2) without sampling or interpolation errors so as to (i) most simply illustrate the nonuniqueness problem, (ii) show that the problem of nonuniqueness could potentially occur even with the most optimistic data quality and spatial coverage scenarios, and (iii) verify that the main components of our numerical codes for the iterative Gal-Chen procedure and our proposed technique are free of errors. Now consider an analyzed reflectivity field valid at any time t between the two CAPPI times of the form

$$R = A \exp[-(ky)^2] \cos[k(x - Ut)], \tag{5.3}$$

with the pattern advection components analyzed as the constant values

$$U = U_{\text{true}} + \frac{2\pi m}{kT}, \quad V = 0, \tag{5.4}$$

TABLE 1. Pattern-translation components U and V from a Gal-Chen-like retrieval and from the spatially variable procedure with $\beta = 10\ \mathrm{dB}Z^2$. The input reflectivity data satisfy (5.2) with parameter values given in the text. Tests were conducted using three sets of first guesses for U and V. The true values of U and V are -15 and 0 m s^{-1}, respectively. All values are in meters per second.

First guesses	Gal-Chen retrieval	Spatially variable retrieval
Test 1: $U \simeq 6.412$, $V \simeq 0.000$	$U \simeq 5.035$, $V \simeq 0.000$	$5.038 < U < 5.062$, $-0.004 < V < 0.004$
Test 2: $U = 0$, $V = 0$	$U \simeq 5.035$, $V \simeq 0.000$	$5.004 < U < 5.037$, $-0.004 < V < 0.004$
Test 3: $U = -10$, $V = -10$	$U \simeq -15.049$, $V \simeq 0.000$	$-15.052 < U < -14.981$, $-0.020 < V < 0.027$

where m is any integer. It is easy to show that (5.3) satisfies the two data constraints [(5.2)]. Moreover, since (5.3) exactly satisfies the advection Eq. (1.2), while all orders of the spatial and temporal derivatives of the analyzed advection fields (5.4) vanish throughout the analysis domain, the cost function defined in (5.1) is zero, which is a minimum value. However, since there is no restriction on m other than it being an integer, there are, in principle, an infinite number of U and corresponding analyzed reflectivity fields that exactly satisfy all conditions of the analysis problem. This example illustrates that the class of advection-correction/analysis procedures governed by (5.1) with data incorporated at two CAPPI times is potentially subject to stroboscopic effects arising from temporal aliasing.

As an illustrative example, we tested an iterative Gal-Chen-like analysis procedure using (5.2) with $A = 10\ \mathrm{dB}Z$, wavelength $\lambda = 6$ km ($k = 2\pi/\lambda$), $T = 300$ s, and $U_{\mathrm{true}} = -15$ m s^{-1}. The analysis domain was a 50 km $\times$ 50 km square with a gridpoint spacing of $\Delta x = \Delta y = 200$ m. The computational time step was $\Delta t = 10$ s. The procedure was deemed to have converged when the U and V fields on all grid points changed by less than 10^{-3} m s^{-1} from their values in the previous iteration. The reflectivity was analyzed along trajectories using (3.10) and (3.11), which, as already noted, provide linear interpolation in the case where U and V are constant. A ''correct'' analysis should yield values of U and V close to those from (5.4) with $m = 0$, that is -15 and 0 m s^{-1}, respectively. Since the y dependence of the reflectivity field is Gaussian rather than wavy, we anticipate that ''incorrect'' analyses would still yield V close to 0 m s^{-1}, but that values of U would be close to those obtained from (5.4) with nonzero values of m. In test 1, the first guesses for U and V were obtained from Gal-Chen's linear algebraic equations with coefficients estimated from reflectivity data that had not been advection corrected (i.e., from a single-pass of the Gal-Chen procedure in which the local derivative was discretized across the scan interval T, and spatial derivatives were discretized as centered spatial differences averaged between times $t = 0$ and $t = T$). The computed first guesses—$U \simeq 6.412$ m s^{-1}, V $\simeq 0.000$ m s^{-1}—were close to the values associated with a wrong ($m = 1$) solution. Not surprisingly, the procedure converged rapidly (three iterations) and with good precision to this wrong solution (Table 1). In test 2, the first guesses for U and V were set to zero. The procedure again converged rapidly (four iterations) to the same wrong solution. In test 3, the first guesses for U and V were set to -10 m s^{-1}. In this case, the procedure converged in six iterations to the correct solution.

Next, we tested the new spatially variable procedure with the same input data, analysis parameters, and first-guess values as described above. During each iteration of the overall procedure, the successive relaxation algorithm ran until changes in the wind components at all grid points were less than 10^{-6} m s^{-1}, or until 40 000 iterations had been completed. The high spatial and temporal resolution of the analysis and the extremely small convergence thresholds for the relaxation algorithm (10^{-6} m s^{-1}) and the overall procedure (10^{-3} m s^{-1}) are probably unnecessarily stringent for most applications, but they were useful here to establish that the main components of the numerical codes were free of errors. For the present case in which the actual advection components are constant and the input data are free of error, one would expect an error-free spatially variable analysis code to yield analyzed winds that are nearly constant on the analysis grid, nearly independent of the value of the smoothness weight β, and very close to one of the solutions given by (5.4). Indeed, tests using the same three sets of first guesses described above yielded U, V fields that were nearly constant (Table 1), with values obtained with $\beta = 10\ \mathrm{dB}Z^2$ very similar to those obtained with $\beta = 100\ \mathrm{dB}Z^2$ (not shown) and to those obtained in the tests of the Gal-Chen procedure.

6. Summary and future work

In this study we considered an advection-correction/analysis procedure for radar reflectivity in which the pattern-advection components vary spatially. The procedure was motivated by the common scenario in which reflectivity features in different parts of a convective storm advect at different speeds. The analysis was phrased as a variational problem in which errors in the frozen-turbulence constraint were minimized

subject to smoothness constraints. The Euler–Lagrange equations for this problem simplified in characteristic coordinates (trajectories), and their solution was proposed through a combined analytical and numerical procedure.

A theoretical analysis of a fairly general class of advection-correction/analysis procedures indicated that the new spatially variable method as well as the Gal-Chen reflectivity-based pattern-advection procedure and some single-Doppler velocity retrievals (e.g., VET) might be susceptible to solution nonuniqueness associated with temporal aliasing. This implies that in real applications the solutions obtained by these methods may sometimes depend on the first guesses for U and V. However, Germann and Zawadzki (2002) suggest that, in practice, an accurate analysis can be obtained if one uses a reasonably accurate first guess. Assuming this is the case, it may be desirable to simply base the first guess on a subjective (visual) estimation of the motion of key features of interest (Heymsfield 1978; Carbone 1982; Austin 1987; Dowell and Bluestein 1997). Confidence in the final results could then be bolstered if the analyses were found to be relatively insensitive to perturbations of the first guess about the visual estimate.

In the future, we would like to extend the present methodology to include time dependence in the pattern-advection components. One possible extension in that direction is outlined in the appendix. It may also be desirable to extend the current methodology to three dimensions by including a vertical advection term in the frozen-turbulence constraint and vertical derivative terms in the smoothness constraint; however, such an extension would require grappling with the problem of interpolating nonsimultaneous data from multiple elevation angles (an issue discussed at the beginning of section 2).

The current version of the spatially variable advection correction procedure was tested using analytical reflectivity blobs embedded in a solid-body vortex and real TDWR and WSR-88D data of a tornadic supercell thunderstorm that passed over central Oklahoma on 8 May 2003. Results from these tests will be reported on in Part II of this study.

Acknowledgments. The authors thank the anonymous reviewers for their helpful comments. This research was supported by the National Science Foundation (NSF) under Grant ATM-0532107, by the Engineering Research Centers Program of the NSF under Cooperative Agreement EEC-0313747, and by the NOAA/NWS Collaborative Science, Technology, and Applied Research (CSTAR) Program through Grant NA17RJ1227.

APPENDIX

Advection Correction of Reflectivity Data with Unsteady Pattern-Advection Fields

The analysis procedure described in this paper applies to U, V advection fields that vary spatially (gradually) but are in a steady state. We now show how the analysis procedure can be extended to include U, V fields that also vary slowly in time (in an Eulerian sense). Consider a new cost function K defined on the analysis surface by

$$K \equiv J + \iiint \left[\gamma \left(\frac{\partial U}{\partial t} \right)^2 + \gamma \left(\frac{\partial V}{\partial t} \right)^2 \right] dx\, dy\, dt, \tag{A.1}$$

where J is defined in (2.1) and γ is a constant positive temporal weighting coefficient. The new cost function differs from the original by inclusion of weak-constraint terms penalizing large temporal derivatives of U, V. When K is minimized, these new terms will provide ''smoothness in time'' for the U, V fields. We view the temporal weight γ as a tunable parameter, as in our treatment of the spatial smoothness weight β.

It can readily be shown that two of the Euler–Lagrange equations corresponding to the minimization of (A.1) are

$$\frac{\gamma}{\beta}\frac{\partial^2 U}{\partial t^2} + \frac{\partial^2 U}{\partial x^2} + \frac{\partial^2 U}{\partial y^2} - \frac{\alpha}{\beta}\left[\frac{\partial R}{\partial t}\frac{\partial R}{\partial x} + U\left(\frac{\partial R}{\partial x} \right)^2 + V\frac{\partial R}{\partial x}\frac{\partial R}{\partial y} \right] = 0 \quad \text{and} \tag{A.2a}$$

$$\frac{\gamma}{\beta}\frac{\partial^2 V}{\partial t^2} + \frac{\partial^2 V}{\partial x^2} + \frac{\partial^2 V}{\partial y^2} - \frac{\alpha}{\beta}\left[\frac{\partial R}{\partial t}\frac{\partial R}{\partial y} + U\frac{\partial R}{\partial x}\frac{\partial R}{\partial y} + V\left(\frac{\partial R}{\partial y} \right)^2 \right] = 0. \tag{A.2b}$$

Equations (A.2a) and (A.2b) are similar to (3.6a) and (3.6b) in that they are elliptic (now in x, y, and t variables), but unlike (3.6a) and (3.6b), the terms involving reflectivity are instantaneous values (i.e., not time integrals), and time derivatives of U, V now appear. The third Euler–Lagrange equation is found to be identical to (3.6c). In the course of deriving these three Euler–Lagrange equations, the same boundary conditions obtained in section 3 are found to apply in this extended case, but we must also impose the temporal conditions $\partial U/\partial t = 0$ and $\partial V/\partial t = 0$ at the two CAPPI times.

Since (3.6c) applies, and we also impose (3.7) on α, all the subsequent analysis formulas in section 3 apply in

the present case as well. The extended procedure differs from that in section 3 in the determination of a time dependence in U, V through the relaxation solution of (A.2a) and (A.2b). The Runge–Kutta formulas used in the trajectory calculations (section 4) should also be adjusted to accommodate the explicit Eulerian unsteadiness in the U, V fields.

REFERENCES

Anagnostou, E. N., and W. F. Krajewski, 1999: Real-time radar rainfall estimation. Part I: Algorithm formulation. *J. Atmos. Oceanic Technol.,* **16,** 189–197.

Andrejczuk, M., S. Moszkowicz, K. Haman, and T. Szoplik, 2003: Radar-echo tracking by use of invariant moments. *Appl. Opt.,* **42,** 5891–5896.

Austin, G. L., and A. Bellon, 1974: The use of digital weather radar records for short-term precipitation forecasting. *Quart. J. Roy. Meteor. Soc.,* **100,** 658–664.

Austin, P. M., 1987: Relation between measured radar reflectivity and surface rainfall. *Mon. Wea. Rev.,* **115,** 1053–1070.

Biggerstaff, M. I., and Coauthors, 2005: The Shared Mobile Atmospheric Research and Teaching Radar: A collaboration to enhance research and teaching. *Bull. Amer. Meteor. Soc.,* **86,** 1263–1274.

Caillault, K., and Y. Lemaitre, 1999: Retrieval of three-dimensional wind fields corrected for the time-induced advection problem. *J. Atmos. Oceanic Technol.,* **16,** 708–722.

Carbone, R. E., 1982: A severe frontal rainband. Part I: Stormwide hydrodynamic structure. *J. Atmos. Sci.,* **39,** 258–279.

Caya, A., S. Laroche, I. Zawadzki, and T. Montmerle, 2002: Using single-Doppler data to obtain a mesoscale environmental field. *J. Atmos. Oceanic Technol.,* **19,** 21–36.

Chong, M., J. Testud, and F. Roux, 1983: Three-dimensional wind field analysis from dual-Doppler radar data. Part II: Minimizing the error due to temporal variation. *J. Climate Appl. Meteor.,* **22,** 1216–1226.

Clarke, T. L., F. I. Harris, and C. G. Mohr, 1980: Errors in wind fields derived from multiple-Dopper radars: Random errors and temporal errors associated with advection and evolution. *J. Appl. Meteor.,* **19,** 1273–1284.

Courant, R., and D. Hilbert, 1953: *Methods of Mathematical Physics*. Vol. 1. Wiley-Interscience, 560 pp.

Crook, A., 1994: Numerical simulations initialized with radar-derived winds. Part I: Simulated data experiments. *Mon. Wea. Rev.,* **122,** 1189–1203.

Crum, T. D., and R. L. Alberty, 1993: The WSR-88D and the WSR-88D Operational Support Facility. *Bull. Amer. Meteor. Soc.,* **74,** 1669–1687.

Dixon, M., and G. Wiener, 1993: TITAN: Thunderstorm Identification, Tracking Analysis and Nowcasting—A radar-based methodology. *J. Atmos. Oceanic Technol.,* **10,** 785–797.

Dowell, D. C., and H. B. Bluestein, 1997: The Arcadia, Oklahoma, storm of 17 May 1981: Analysis of a supercell during tornadogenesis. *Mon. Wea. Rev.,* **125,** 2562–2582.

——, and ——, 2002: The 8 June 1995 McLean, Texas, Storm. Part I: Observations of cyclic tornadogenesis. *Mon. Wea. Rev.,* **130,** 2626–2648.

Fabry, F., A. Bellon, M. R. Duncan, and G. L. Austin, 1994: High resolution rainfall measurements by radar for very small basins: The sampling problem reexamined. *J. Hydrol.,* **161,** 415–428.

Flanigan, F. J., 1983: *Complex Variables*. Dover, 353 pp.

Fulton, R., J. Breidenbach, D.-J. Seo, D. Miller, and T. O'Bannon, 1998: The WSR-88D rainfall algorithm. *Wea. Forecasting,* **13,** 377–395.

Gal-Chen, T., 1978: A method for the initialization of the anelastic equations: Implications for matching models with observations. *Mon. Wea. Rev.,* **106,** 587–606.

——, 1982: Errors in fixed and moving frame of references: Applications for conventional and Doppler radar analysis. *J. Atmos. Sci.,* **39,** 2279–2300.

Gao, J., M. Xue, A. Shapiro, Q. Xu, and K. K. Droegemeier, 2001: Three-dimensional simple adjoint velocity retrievals from single Doppler radar. *J. Atmos. Oceanic Technol.,* **18,** 26–38.

Germann, U., and I. Zawadzki, 2002: Scale-dependence of the predictability of precipitation from continental radar images. Part I: Description of the methodology. *Mon. Wea. Rev.,* **130,** 2859–2873.

Gerstner, E.-M., and G. Heinemann, 2008: Real-time areal precipitation determination from radar by means of statistical objective analysis. *J. Hydrol.,* **352,** 296–308.

Hane, C. E., 1993: Storm-motion estimates derived from dynamic-retrieval calculations. *Mon. Wea. Rev.,* **121,** 431–443.

——, R. B. Wilhelmson, and T. Gal-Chen, 1981: Retrieval of thermodynamic variables within deep convective clouds: Experiments in three dimensions. *Mon. Wea. Rev.,* **109,** 564–576.

Heymsfield, G. M., 1978: Kinematic and dynamic aspects of the Harrah tornadic storm analyzed from dual-Doppler radar data. *Mon. Wea. Rev.,* **106,** 233–254.

Islam, M. R., and P. F. Rasmussen, 2008: Improved high-resolution radar-based rainfall estimation. *J. Hydrol. Eng.,* **13,** 910–913.

Johnson, J., P. MacKeen, A. Witt, E. Mitchell, G. Stumpf, M. Eilts, and K. Thomas, 1998: The storm cell identification and tracking algorithm: An enhanced WSR-88D algorithm. *Wea. Forecasting,* **13,** 263–276.

Klazura, G. E., and D. A. Imy, 1993: A description of the initial set of analysis products available from the NEXRAD WSR-88D system. *Bull. Amer. Meteor. Soc.,* **74,** 1293–1311.

Lakshmanan, V., R. Rabin, and V. DeBrunner, 2003: Multiscale storm identification and forecast. *Atmos. Res.,* **67–68,** 367–380.

——, T. Smith, K. Hondl, G. J. Stumpf, and A. Witt, 2006: A real-time, three-dimensional, rapidly updating, heterogeneous radar merger technique for reflectivity, velocity, and derived products. *Wea. Forecasting,* **21,** 802–823.

Lanczos, C., 1986: *The Variational Principles of Mechanics*. Dover, 418 pp.

Langston, C., J. Zhang, and K. Howard, 2007: Four-dimensional dynamic radar mosaic. *J. Atmos. Oceanic Technol.,* **24,** 776–790.

Laroche, S., and I. Zawadzki, 1995: Retrievals of horizontal winds from single-Doppler clear-air data by methods of cross correlation and variational analysis. *J. Atmos. Oceanic Technol.,* **12,** 721–738.

Lazarus, S., A. Shapiro, and K. Droegemeier, 2001: Application of the Zhang–Gal-Chen single-Doppler velocity retrieval to a deep convective storm. *J. Atmos. Sci.,* **58,** 998–1016.

Liou, Y.-C., 1999: Single radar recovery of cross-beam wind components using a modified moving frame of reference technique. *J. Atmos. Oceanic Technol.,* **16,** 1003–1016.

——, 2001: The derivation of absolute potential temperature perturbations and pressure gradients from wind measurements in three-dimensional space. *J. Atmos. Oceanic Technol.,* **18,** 577–590.

——, and I.-S. Luo, 2001: An investigation of the moving-frame single-Doppler wind retrieval technique using Taiwan Area Mesoscale Experiment low-level data. *J. Appl. Meteor.,* **40,** 1900–1917.

Liu, C., and W. F. Krajewski, 1996: A comparison of methods for calculation of radar-rainfall hourly accumulations. *Water Resour. Bull.,* **32,** 305–315.

Liu, S., C. Qiu, Q. Xu, and P. Zhang, 2004: An improved time interpolation for three-dimensional Doppler wind analysis. *J. Appl. Meteor.,* **43,** 1379–1391.

Lu, H., and Q. Xu, 2009: Trade-offs between measurement accuracy and resolutions in configuring phased-array radar velocity scans for ensemble-based storm-scale data assimilation. *J. Appl. Meteor. Climatol.,* **48,** 1230–1244.

Matejka, T., 2002: Estimating the most steady frame of reference from Doppler radar data. *J. Atmos. Oceanic Technol.,* **19,** 1035–1048.

Michelson, M., W. W. Shrader, and J. G. Wieler, 1990: Terminal Doppler weather radar. *Microwave J.,* **33,** 139–148.

Miller, L. J., and R. A. Kropfli, 1980: The multiple Doppler radar workshop, November 1979. Part II: Experimental design and procedures. *Bull. Amer. Meteor. Soc.,* **61,** 1173–1177.

Mohr, C. G., L. J. Miller, R. L. Vaughan, and H. W. Frank, 1986: The merger of mesoscale datasets into a common Cartesian format for efficient and systematic analyses. *J. Atmos. Oceanic Technol.,* **3,** 143–161.

NOAA/NWS, 2005: TDWR interface control and specifications documentation for the NWS supplemental product generator, version 4.3, 42 pp. [Available online at http://wdtb.noaa.gov/buildTraining/TDWR/TDWR_SPG_ICD_v43.pdf.]

Parsons, D. B., C. G. Mohr, and T. Gal-Chen, 1987: A severe frontal rainband. Part III: Derived thermodynamic structure. *J. Atmos. Sci.,* **44,** 1615–1631.

Press, W. H., S. A. Teukolsky, W. T. Vetterling, and B. P. Flannery, 1992: *Numerical Recipes in FORTRAN: The Art of Scientific Computing*. 2nd ed. Cambridge University Press, 963 pp.

Protat, A., and I. Zawadzki, 1999: A variational method for real-time retrieval of three-dimensional wind field from multiple-Doppler bistatic radar network data. *J. Atmos. Oceanic Technol.,* **16,** 432–449.

Ray, P. S., M. Gilet, and K. W. Johnson, 1980: The multiple Doppler radar workshop, November 1979. Part IV: Motion field synthesis and radar placement. *Bull. Amer. Meteor. Soc.,* **61,** 1184–1189.

Rosenfeld, D., 1987: Objective method for analysis and tracking of convective cells as seen by radar. *J. Atmos. Oceanic Technol.,* **4,** 422–434.

Roux, F., 1985: Retrieval of thermodynamic fields from multiple-Doppler radar data using the equations of motion and the thermodynamic equation. *Mon. Wea. Rev.,* **113,** 2142–2157.

Sasaki, Y., 1970: Some basic formalisms in numerical variational analysis. *Mon. Wea. Rev.,* **98,** 875–883.

——, 1971: A theoretical interpretation of anisotropically weighted smoothing on the basis of numerical variational analysis. *Mon. Wea. Rev.,* **99,** 698–707.

Shapiro, A., S. Ellis, and J. Shaw, 1995: Single-Doppler velocity retrievals with Phoenix II data: Clear air and microburst wind retrievals in the planetary boundary layer. *J. Atmos. Sci.,* **52,** 1265–1287.

——, P. Robinson, J. Wurman, and J. Gao, 2003: Single-Doppler velocity retrieval with rapid scan radar data. *J. Atmos. Oceanic Technol.,* **20,** 1758–1775.

——, K. M. Willingham, and C. K. Potvin, 2010: Spatially variable advection correction of radar data. Part II: Test results. *J. Atmos. Sci.,* **67,** 3457–3470.

Sun, J., and R. A. Houze Jr., 1992: Validation of a thermodynamic retrieval technique by application to a simulated squall line with trailing stratiform precipitation. *Mon. Wea. Rev.,* **120,** 1003–1018.

——, and N. A. Crook, 1994: Wind and thermodynamic retrieval from single-Doppler measurements of a gust front observed during Phoenix II. *Mon. Wea. Rev.,* **122,** 1075–1091.

——, and ——, 2001: Real-time low-level wind and temperature analysis using single WSR-88D data. *Wea. Forecasting,* **16,** 117–132.

Tabary, P., 2007: The new French operational radar rainfall product. Part I: Methodology. *Wea. Forecasting,* **22,** 393–408.

Taylor, G. I., 1938: The spectrum of turbulence. *Proc. Roy. Soc. London,* **164A,** 476–490.

Tuttle, J. D., and G. B. Foote, 1990: Determination of the boundary layer airflow from a single Doppler radar. *J. Atmos. Oceanic Technol.,* **7,** 218–232.

Vasiloff, S. V., 2001: Improving tornado warnings with the Federal Aviation Administration's terminal Doppler weather radar. *Bull. Amer. Meteor. Soc.,* **82,** 861–874.

Villarini, G., and W. F. Krajewski, 2010: Review of the different sources of uncertainty in single-polarization radar-based estimates of rainfall. *Surv. Geophys.,* **31,** 107–129.

Wurman, J., J. Straka, E. Rasmussen, M. Randall, and A. Zahrai, 1997: Design and deployment of a portable, pencil-beam, pulsed, 3-cm Doppler radar. *J. Atmos. Oceanic Technol.,* **14,** 1502–1512.

Xu, Q., H. Gu, and C. Qiu, 2001a: Simple adjoint retrievals of wet-microburst winds and gust-front winds from single-Doppler radar data. *J. Appl. Meteor.,* **40,** 1485–1499.

——, ——, and S. Yang, 2001b: Simple adjoint method for three-dimensional wind retrievals from single-Doppler radar. *Quart. J. Roy. Meteor. Soc.,* **127,** 1053–1067.

Yang, H., J. Zhang, and C. Langston, 2009: Synchronization of radar observations with multi-scale storm tracking. *Adv. Atmos. Sci.,* **26,** 78–86.

Zawadzki, I. I., 1973: Statistical properties of precipitation patterns. *J. Appl. Meteor.,* **12,** 459–472.

Zhang, J., and T. Gal-Chen, 1996: Single-Doppler wind retrieval in the moving frame of reference. *J. Atmos. Sci.,* **53,** 2609–2623.

Zrnic, D. S., and Coauthors, 2007: Agile-beam phased array radar for weather observations. *Bull. Amer. Meteor. Soc.,* **88,** 1753–1766.